Materials Today Bio 32 (2025) 101752

Contents lists available at ScienceDirect

Materials Today Bio

journal homepage: www.journals.elsevier.com/materials-today-bio

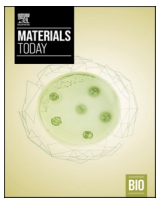

Transdermal delivery of timolol maleate using hydrogel microneedles for the treatment of infantile haemangiomas☆

Xiaokun Lin [a,b,c,1], Tongshuai Kuang [a,b,c,1], Lei Wang [b,d,*,1], Wei Cai [a], Linxing Yang [c], Changrong Guo [c], Xinyang Pan [c], Yuanhao Wang [c], Qiang Gao [b], Kaihui Nan [b,**], Lingli Li [b,c,***]

[a] Department of Pediatric Surgery, The Second Affiliated Hospital and Yuying Children's Hospital, Wenzhou Medical University, Wenzhou, Zhejiang, 325027, China
[b] Wenzhou Key Laboratory of Biomaterials and Engineering, Wenzhou Institute, University of Chinese Academy of Sciences, Wenzhou, Zhejiang, 325000, China
[c] State Key Laboratory of Eye Health, Eye Hospital, Wenzhou Medical University, Wenzhou, Zhejiang, 325027, China
[d] The Affiliated Xiangshan Hospital, Wenzhou Medical University, Ningbo, Zhejiang, 315700, China

ARTICLE INFO

Keywords:
Transdermal drug delivery systems
Infantile haemangioma
Hydrogel microneedles
Bovine serum albumin methacryloyl
Timolol maleate

ABSTRACT

Infantile haemangioma (IH), the most prevalent vascular tumour in infants, requires early intervention because of the potential complications in critical areas such as the head and face. Current treatments, including topical timolol maleate (TIM), face challenges such as poor compliance, low drug utilisation, and lengthy treatment durations. In this study, we developed a hydrogel microneedle (MN) using photocurable bovine serum albumin methacryloyl (BSAMA) as a carrier for TIM. Our results showed the controlled release of TIM from BSAMA-TIM MNs, with approximately 69 % release ratio within 72 h. *In-vivo* studies on nude mice demonstrated that BSAMA-TIM-MNs inhibited the growth of haemangioma xenografts. Our TIM-delivering MNs exhibited high therapeutic efficacy, minimal cytotoxicity, and reduced dosing frequency. In conclusion, BSAMA-TIM MNs provide a promising strategy for treating IH.

1. Introduction

Infantile haemangioma (IH), with a prevalence of 4–5 %, is the most common benign tumour in infants [1]. It predominantly affects females, Caucasians, infants with low birth weights, and premature infants [2]. Although its exact aetiology remains elusive, IH is recognised as a disorder of angiogenesis and vasculogenesis marked by excessive microvascular proliferation [3]. IH typically exhibits a characteristic growth pattern featuring a rapid proliferative phase followed by spontaneous involution [4]. Ulceration is an important complication of IHs, with an incidence of 15–30 % [5]. In addition, approximately 10 % of patients with untreated IH may develop telangiectasias, scarring, skin atrophy, and fibrofatty residues, leading to potential risks of disfigurement and functional impairment. Therefore, there is an urgent need to develop effective management strategies for IH [6].

The current treatments for IH include systemic medications, topical treatments, and surgical interventions [7]. For instance, oral administration of propranolol is a common systemic treatment. however, its frequent use has potential risk of inducing acute kidney injury and damaging the gastrointestinal tract due to its toxic side effects and large drug dosage. Besides, it is reported with side effects such as bradycardia, bronchospasm, hypotension, hypoglycaemia, electrolyte disturbances, diarrhoea, and even potential long-term neurocognitive and neurological developmental repercussions owing to the high blood-brain barrier penetration of propranolol [8,9]. Clinical studies have shown that propranolol also causes central nervous system symptoms, such as drowsiness or sleep disturbances [10]. However, there is no conventional method for evaluating its impact on neurological development [11].

Timolol, a potent non-selective β-receptor antagonist, blocks both β1 and β2 receptors and has a pharmacological potency that is tenfold that

☆ We affirm that this study adheres to ethical standards and guidelines, and all authors have contributed to the research and preparation of the manuscript.

* Corresponding author. Jinlian Road #1, Wenzhou, Zhejiang, China.
** Corresponding author. Xueyuan West Road #270, Wenzhou, Zhejiang, China.
*** Corresponding author. Xueyuan West Road #270, Wenzhou, Zhejiang, China.
E-mail addresses: wanglei20111213@ucas.ac.cn (L. Wang), nankh@163.com (K. Nan), Lingli_lee@yeah.net (L. Li).
[1] These authors contributed equally to this work.

https://doi.org/10.1016/j.mtbio.2025.101752
Received 12 December 2024; Received in revised form 29 March 2025; Accepted 9 April 2025
Available online 12 April 2025

of propranolol. Initially used in 1978 for glaucoma treatment, subsequent studies have confirmed the safety of timolol in paediatric populations [12,13]. As an ophthalmic agent, timolol exerts minimal local tissue irritation and yields negligible systemic absorption, thus minimising systemic effects [14–16]. In 2010, Guo et al. reported the efficacy of topical 0.5 % timolol maleate eye drops in eyelid haemangioma treatment, which led to a significant increase in reports on its application for treating IHs [13,17–19]. However, the utilisation rate of topical timolol remains low, and its short-term therapeutic efficacy is limited. Studies have suggested that simply increasing the dosage does not improve efficacy, leading to the hypothesis that enhancing the transdermal delivery efficiency could significantly augment its therapeutic effects [20–22]. Moreover, maintaining stable local drug concentrations is a critical clinical requirement for IH treatment, avoiding underdosing (inefficacy) or overdosing (toxicity), especially in sensitive pediatric populations [23].

The skin acts as the primary barrier to topical drug delivery and comprises three main layers, the stratum corneum, epidermis, and dermis, arranged from the outermost to the innermost layers. The stratum corneum plays a pivotal role by selectively allowing the passage of molecules, especially lipophilic molecules with low molecular weights [24]. The thickest part of the epidermis of normal adults is approximately 596.6 μm thick, while that of infants (aged 3–24 months) is approximately 20–30 % thinner [25,26]. Conventional transdermal drug delivery methods, such as transdermal patches, chemical permeation enhancers, topical formulations, have inherent limitations [27]. For example, topical creams typically remain superficial, and studies shows that only a small fraction (10–20 %) of the drug content penetrates the skin [28]. Transdermal patches face difficulties delivering drugs across the stratum corneum, leading to suboptimal drug utilisation. Although incorporating penetration enhancers into transdermal patches can improve drug permeability, the extent of this improvement is often limited [29]. Subcutaneous injections, although effective in delivering drugs through the skin, cause discomfort to patients and are particularly unsuitable for infants and young children. Thus, improving the transdermal permeability of timolol and optimising its therapeutic efficacy are challenging.

Microneedle (MN) technology is a promising method to enhance drug permeation across the skin barrier [30]. Hydrogel microcarriers have high efficiency, softness, biocompatibility, superior drug-loading capacity, and sustained-release ability, which ensure optimal drug levels in the body, and are emerging as noteworthy candidates for drug delivery [31–33]. Materials used for preparing hydrogel microneedles can be categorized into different types. Among them, synthetic polymers like Poly (methyl vinyl ether-alt-maleic anhydride) (PMVE/MA), polyvinyl alcohol (PVA), and Polystyrene-block-Polyacrylic acid (PS-b-PAA)) are often utilised. These synthetic polymers offer advantages such as adjustable properties through molecular design, which can contribute to the desired mechanical strength of the hydrogel microneedles. On the other hand, natural materials such as Methylated Hyaluronic Acid (MeHA) and Gelatin methacryloyl (GelMA) are also popular choices [34,35]. Natural materials generally possess good biosafety profiles due to their origin and compatibility with biological systems. In recent years, protein-based hydrogel materials have attracted increasing attention from scientists. They possess excellent biocompatibility and exhibit outstanding mechanical strength after light-induced crosslinking, which is crucial for inserting microneedles into the skin. The combination of mechanical properties and biocompatibility makes protein-based materials stand out among other options and holds great potential for the development of advanced hydrogel microneedle systems [36,37].

As the most abundant plasmatic protein-derived material, bovine serum albumin methacryloyl (BSAMA) is prepared by replacing the hydroxyl groups in the bovine serum albumin (BSA) backbone with methacrylate groups, followed by UV crosslinking. The fractional helicity, amide bands, and secondary structure of BSA are widely used in tissue engineering [38–40]. BSAMA has a secondary structure similar to that of BSA, and most of its metabolites are natural amino acids, indicating its excellent biocompatibility [41,42]. Studies have shown that BSAMA supports *in vitro* cell proliferation, maintains cell viability >95 %, and exhibits no haemolytic properties [43]. BSAMA exhibits tuneable physiological properties, such as mechanical performance and microstructures [44,45], which allow the tips of BSAMA-based MNs to pierce the skin without eliciting excessive immunogenicity. PVA is widely used in biomedical hydrogel fabrication because of its biocompatibility, cost-effectiveness, and biodegradability [46,47]. This shows promise for use in MNs fabrication [48]. The dry annealing technique enhances the mechanical strength of PVA hydrogels via physical cross-linking, which is advantageous for preparing MNs substrates with good flexibility [49].

In this study, we developed a hydrogel MNs system as a drug depot for the delivery of timolol maleate (TIM) for IH therapy. BSAMA was utilised as a reservoir for TIM, and PVA served as a substrate material. We investigated the morphological structure, mechanical properties, *in vitro* biocompatibility, release kinetics, and *in vivo* therapeutic potential of BSAMA-TIM-MNs.

2. Materials and methods

2.1. Materials

Timolol maleate (TIM; CAS No.: 26921-17-5) was purchased from MedChemExpress (USA), PVA (CAS No.: 9002-89-5) was purchased from Ourchem (China), BSAMA was purchased from Wenzhou Shuhe Biotechnology Co., LTD (China), and 2-hydroxy-4'-(2-hydroxyethoxy)-2-methylpropiophenone (I2959, CAS No.: 106797-53-9) was purchased from Sigma-Aldrich (USA). Rabbit monoclonal antibody for glucose transporter GLUT1 (ab115730) and mouse monoclonal [JC/70A] antibody for CD31 (ab9498) were purchased from Abcam (USA). Anhydrous dimethyl sulfoxide (DMSO), high-glucose Dulbecco's modified Eagle medium (high-glucose DMEM), and a CCK-8 detection kit were purchased from Sigma Aldrich (USA). Fetal bovine serum (FBS), antibiotics (penicillin/streptomycin), phosphate-buffered saline (PBS), and an annexin V-FITC apoptosis detection kit were purchased from Thermo Fisher Scientific (USA). Mouse uric acid and mouse aspartate aminotransferase enzyme-linked immunoassay kits were purchased from Wuhan Moshak Biotechnology Co., LTD (China). The positive MNs mould was purchased from BMF Precision Tech, Inc. (Shenzhen, China). The SYLGARD 184 Silicone Elastomer Kit was purchased from Dow Inc (USA). Matrigel matrix high concentration was purchased from Corning (USA).

2.2. Preparation and morphological characterisation of negative MNs mould

Positive MNs moulds made of high-precision photosensitive resin (15 × 15 arrays, needle height of 600 μm) were positioned at the bottom of the central holes in a 12-well plate, ensuring central alignment without contact with the sidewalls. The two liquids from the Silicone Elastomer Kit were thoroughly mixed in a 10:1 ratio. The well-mixed Dow silicone encapsulant was poured into the holes containing the MN tips to ensure that the liquid covered the tips by > 1 cm. A high-speed centrifuge (4 °C, 4000 rpm, 3 min) was used to remove bubbles around the MN tips. Subsequently, the plate was placed on a heating platform at 80 °C for 2 h to cure the silicone. The surface morphology of the resulting MN tips was characterised by optical microscopy (JSZ6S, Jiangnan Novel Optics) and scanning electron microscopy (SEM, SU8010, Hitachi, Japan).

2.3. Preparation and morphological characterisation of BSAMA–MNs and BSAMA-TIM-MNs

A prepolymer solution for the MNs was prepared using a mixture of

10 % (w/v) BSAMA and 0.5 % (w/v) I2959. The mixed solution (200 μL) was added to a negative MNs mould. The mould was then subjected to vacuum pumping to remove any bubbles and ensure that the solution completely filled the cavities. The mould was then placed in a drying oven for 45 min to thicken the mixture. UV light was applied vertically to the prepolymer solution in the Polydimethylsiloxane (PDMS) mould for 10 min to solidify the BSAMA-MNs. 200 μL of 10 % PVA solution was added to the negative MN mould, and then, the mould was placed in the drying oven at 37° overnight. The MNs were carefully peeled from the PDMS mould. For the preparation of BSAMA-TIM-MNs, TIM powder was added to a mixture of BSAMA and I2959 at a concentration of 9 mg/mL. Ultrasound was used to aid in dissolution and mixture. The prepared BSAMA-MN patches comprised 15 × 15 arrays of pyramidal needles. The base of each needle was 300 μm wide and 600 μm long. Finally, the surface morphology of the BSAMA-MNs was observed using optical microscopy and SEM.

2.4. Mechanical performance of BSAMA–MNs and BSAMA-TIM-MNs

The mechanical properties of BSAMA-MNs and BSAMA-TIM-MNs were assessed using a universal pressure testing machine (5944, Instron). The MNs patches were positioned horizontally on a stable base with the needle tips facing upward. The force sensor was slowly brought closer to the MNs in the vertical direction. The sensor descended at a rate of 0.2 mm/s, and measurements were taken when the sensor contacted the MN tips. The measurements continued until the pressure on the sensor reached 100 N. This process was repeated for five patches loaded with TIM.

2.5. In vitro drug release

We used a Franz diffusion cell to evaluate the *in vitro* drug release capability of BSAMA-TIM-MNs and determine the drug release profile of the MNs patch. The Franz diffusion cell consisted of a supply chamber and a receiving chamber separated by a layer of nude mouse skin. The normal microenvironment around the haemangioma tissue *in vivo* was simulated using a constant temperature layer heated on the outside by 37 °C circulating water. After assembling the device, 80 mL of PBS was added to the receiving tank, and a rotor was introduced to stir at 300 rpm. BSAMA-TIM-MNs were then applied to the epidermis of nude mice using 5 N pressure for 30 s, which allowed the MNs to penetrate the epidermis and initiate drug release. The control group was treated with topical application of timolol maleate (Free TIM), simulating the clinical treatment approach. The samples were collected at predetermined time points (2, 4, 8, 10, 12, 24, 48, 72, 96, and 168 h after application). At each time point, 4 mL of the solution was withdrawn from the receiving tank and replaced with an equal volume of PBS. The concentration of TIM in the receiving chamber was quantified by high-performance liquid chromatography (HPLC). Finally, a concentration profile of TIM in the receiving pool was constructed to compare the *in vitro* drug release behaviour of BSAMA-TIM-MNs and Free TIM.

2.6. In vivo drug release

Male nude mice aged 4–5 weeks were selected and housed in a specific pathogen-free (SPF) animal laboratory. After one week of acclimatization, the mice were randomly divided into two groups: a traditional timolol maleate topical application group (Free TIM) and a hydrogel microneedle patch group (BSAMA-TIM-MNs). The BSAMA-TIM-MNs group applied the hydrogel microneedle patch on the back of nude mice, while the Free TIM group used 4 layers of gauze soaked with timolol maleate solution for external application on the same area of nude mice. At 6, 12, 24, 48, and 72 h post-administration, the microneedle patches and gauzes were collected, cut into small pieces, immersed and stirred in 5 mL of PBS buffer pre-warmed to 37 °C for 24 h. Simultaneously, the nude mice were euthanized by isoflurane inhalation anesthesia, and a 1×1 cm section of skin from the administration site was rapidly collected. The collected skin tissue was minced, homogenized, and immersed in 5 mL of PBS buffer pre-warmed to 37 °C for 24 h. The concentrations of TIM in the two extract solutions were determined by ultra-high performance liquid chromatography (UPLC), and then the remaining amounts of TIM in the microneedles and gauze, as well as the deposited amounts of TIM in the skin of nude mice were calculated. Based on the results, obtained the release amount-time graph of TIM *in vivo*, and analyze its release kinetics and tissue distribution.

2.7. Drug stability

To evaluate the stability of timolol maleate within the microneedles, the prepared hydrogel microneedles were stored under three distinct temperature conditions (−20 °C, 4 °C, and 25 °C) for 30 days. Following the storage period, the microneedles were cut into pieces and ground. Then, they were immersed in 10 mL of pre-warmed PBS solution (37 °C) under continuous stirring for 24 h to facilitate drug extraction. The resulting solution was then filtered through a 0.22 μm microporous membrane, and the concentration of timolol maleate in the filtrate was quantified using UPLC. The drug retention rate was subsequently calculated to evaluate the influence of varying storage temperatures on the stability of the drug.

2.8. In vitro cytocompatibility

L929 cells (Cell Bank of the Chinese Academy of Sciences, Shanghai, China) were cultured in high-glucose DMEM supplemented with 10 % (v/v) FBS and 1 % (v/v) penicillin-streptomycin in a cell culture incubator (37 °C, 5 % CO_2). Then, a 2 mL mixture of 15 % (w/v) BSAMA and 0.5 % (w/v) I2959 was added to a 6-well plate, which was then exposed to UV light with a wavelength of 365 nm for 10 min to induce solidification. Subsequently, 1.6 mL of high-glucose DMEM complete culture medium was added to each well and incubated for 72 h, in accordance with the national standards for extracts. L929 cells were seeded in a 96-well plate (5000 cells/well) and cultured in BSAMA extract or DMEM high-glucose complete medium (control) for 5 days, with medium changes occurring every other day. On days 1, 3, and 5 of the experiment, the original culture medium in the well was aspirated, and 100 μL of complete culture medium containing 10 % (v/v) CCK-8 solution was added. The plates were incubated for 3 h in the incubator. The absorbance (OD) at 450 nm was measured using a microplate reader. Simultaneously, the two groups were stained with Live/Dead™ Viability/Cytotoxicity Kit to determine the cell viability. Then, 2 μM calcein AM and 4 μM EthD-1 were added into each well, and cells were cultured in the dark for 30 min. L929 cell viability and morphology were observed using an inverted fluorescence microscope.

2.9. In vitro drug inhibition concentration

In the 2D culture of HemECs, we first seeded HemECs in 96-well plates and cultured it in complete medium for 24 h. Then the culture medium was removed, and cells were exposed to serum-free medium containing different TIM concentrations (10 μM, 100 μM, 1 mM, and 10 mM). At 24 and 48 h, 100 μL of serum-free medium containing 10 % CCK-8 was added to each well, and the cells were cultured in the incubator for 3 h. The absorbance at 450 nm was measured using a microplate reader. In the 3D culture system of HemECs, we resuspended HemECs in Matrigel matrix and added them to 96-well plates. The cells were then cultured in complete medium for 24 h. After that, the complete medium was removed and the cells were exposed to serum-free medium containing different concentrations of TIM (600 μM, 900 μM, 1200 μM, and 1500 μM). At 24 h later, the absorbance at 450 nm was also detected by the CCK-8 method. Another plates of 3D cultured HemECs was subjected to a live/dead staining assay. The cells were cultured in an incubator for 30 min, and the morphology of the HemECs

was observed using an inverted fluorescence microscope.

2.10. In vivo animal experiments

Male nude mice weighing 16–18 g and aged approximately 4–5 weeks were procured from Zhejiang Vital River Laboratory Animal Technology Co., Ltd. The mice were housed under standard conditions that adhered to the regulatory standards and were maintained in a pathogen-free animal facility. To establish an animal model of IH, a mixture of 2×10^6 HemECs and 1×10^6 HUVECs were suspended in 200 μL of Matrigel matrix and injected into the backs of the nude mice. The body weight and the size of the back IH were measured every 3 days, starting from 2 weeks after the initial injection. At 15 days post-subcutaneous injection, nude mice with IH were randomly assigned to four groups: control, TIM external application (Free TIM), blank MNs (BSAMA–MNs), and TIM MNs (BSAMA-TIM-MNs). Each group consisted of seven mice, and the control group received no treatment. In the Free TIM group, 0.5 % TIM eye drops were applied to 1–2 layers of gauze and placed on the tumour surface three times a day, at intervals of 6–8 h, with a dose of 40 μL/cm^2, which mimicked current clinical topical IH treatments. The BSAMA–MNs group received treatment with blank MNs, and the MNs patch was changed every 3 days. The BSAMA-TIM-MNs group was treated using MNs loaded with TIM, and the MNs patch was changed every 3 days. The body weights of all groups were measured every 3 days, and the tumour dimensions (length [L], width [W], and height [H]) on the backs of the nude mice were measured using Vernier callipers. The IH volume was calculated using the following formula: $\pi/6 \times L \times W \times H$. After 2 weeks of treatment, the animals were euthanized by intraperitoneal injection of elevated concentrations of sodium pentobarbital solution, and the IH tissue was extracted for immunohistochemical analysis and protein purification. Vital organs (heart, liver, spleen, lungs, and kidneys) and blood samples from each group were preserved for toxicity analysis. All animal experiments in this study were approved by the Animal Ethics Committee of Wenzhou Medical University (wydw2023-0098). All methods were performed in accordance with ARRIVE guidelines and regulations.

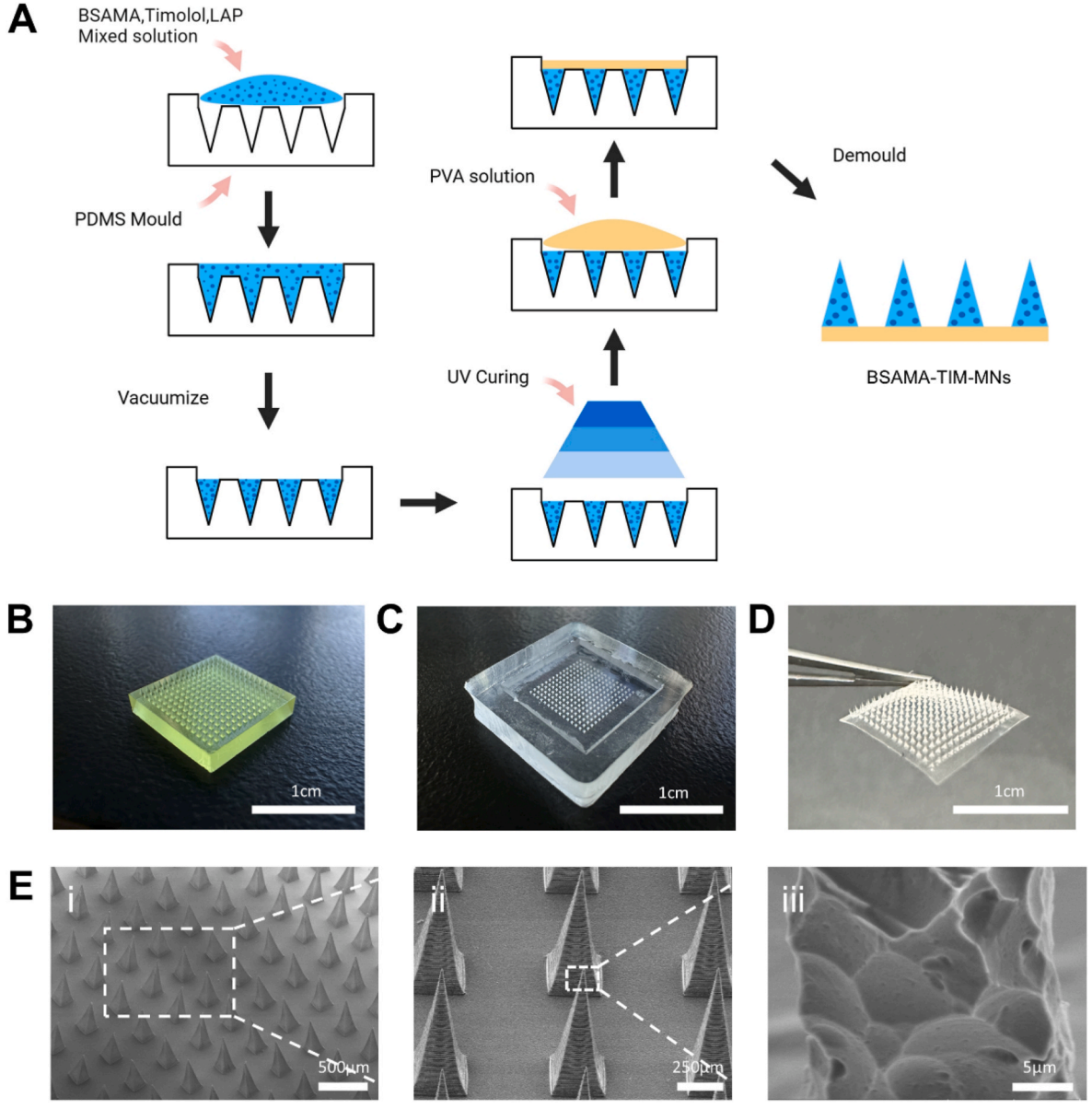

Fig. 1. Preparation and characterization of BSAMA-TIM-MNs. A) Production of BSAMA-TIM-MNs; **B)** Negative mould for MNs made of PDMS. Scale bars: 1 cm; **C)** Positive MNs mould made of high-precision photosensitive resin. Scale bars: 1 cm; **D)** Image of BSAMA-TIM-MNs. Scale bars: 1 cm; **E)** Micromorphology of BSAMA-TIM-MNs using SEM. Scale bars: 500 μm (i), 250 μm (ii), 5 μm (iii).

2.11. Data analysis

Data are expressed as mean ± standard deviation and were analysed using GraphPad Prism (version 8; GraphPad Software, Inc., La Jolla, CA, USA). Differences in means between and among groups were analysed using t-tests and one-way analysis of variance (ANOVA). The levels of significance were set at *p ≤ 0.05, **p ≤ 0.01, and ***p ≤ 0.001.

3. Results

3.1. Preparation and characterisation of MNs patches

BSAMA-TIM-MNs were synthesised by combining vacuuming drying and UV cross-linking (Fig. 1A). The MNs patch was easily removed from the mould with good flexibility (Fig. 1B–D). A representative image of the microneedles (15 × 15 array) is shown in Fig. 1E. The microneedles had sharp tips and well-defined edges. The tetra-pyramidal needles were uniformly and regularly arranged on the surface of the PVA substrate. The average tip diameter was 10 μm, tip height was 600 μm, and bottom edge length was 300 μm. These dimensions closely mirrored the positive and negative templates (Fig. 1B and C), affirming that the MNs maintained their original shape and sharpness throughout processing.

The effect of drug loading on the MNs mechanical strength was investigated by testing the maximum compressive force of the MN, both with and without TIM. Representative force curves of the MNs are shown in Fig. 2A. The failure forces for the BSAMA-MNs and BSAMA-TIM-MNs patches were 144 ± 15.75 and 141 ± 8.51 mN/needle, respectively (Fig. 2B).

We evaluated the skin penetration ability of the MNs by conducting tests on nude mouse skin. The MNs created noticeable microchannels on the surface of the back skin of the nude mice (Fig. 2C). The epidermis of nude mice treated with MNs was stained with haematoxylin & eosin (H & E) and compared with normal epidermis. Obvious defects at regular intervals were observed, with a depth of approximately 200–300 μm (Fig. 2D). These findings strongly suggest successful penetration of the epidermal layer by the MNs, thus enabling effective drug delivery to the dermis.

3.2. In vitro release

The drug release profile of BSAMA-TIM-MNs was evaluated using a Franz diffusion cell setup (Fig. 3A). The dorsal skin of the nude mice acted as a barrier between the donor and recipient compartments. The TIM concentration in the receptor compartment was measured using UPLC. The release of TIM was calculated using a standard curve (Fig. 3B). The release profile exhibited a slow-fast-slow-release pattern (Fig. 3D). Initially, the TIM concentration of MNs gradually increased over the first 12 h, with a cumulative release rate of 4.4 ± 1.0 %. The concentration of MNs rapidly increased, resulting in a total release of 24.1 ± 3.84 % (0.60 ± 0.10 mg) within 24 h. The TIM release continued, with more than half of the loaded amount released at the end of 48 h, reaching 52.61 ± 2.39 % (1.32 ± 0.06 mg). At 72 h, the drug release from the MNs reached 69.02 ± 2.78 % (1.73 ± 0.75 mg), which has already surpassed three times that of the control group. Approximately 80 % of drug release in MNs was released at 96 h, and 90 % was released at 7 days. The morphological changes of the MN tips at various time points during drug release are illustrated in Fig. 3C. Notably, after 7 days, the BSAMA tips degraded, leaving only the smooth PVA substrate (Fig. 3B). The release kinetics of MNs was analysed (Fig. 3E and F) and discussed in the Discussion.

3.3. In vivo release

In vivo sustained-release kinetics were systematically validated through complementary metrics: residual drug quantification in retrieved BSAMA-TIM-MNs and TIM accumulation within dorsal skin tissues of nude mice, providing dual-axis confirmation of controlled drug release patterns. As shown in Fig. 3G, similar to the *in vitro* release, the release of timolol maleate from BSAMA-TIM-MNs was slow during the first 12 h, followed by a significant increase in the release rate over the next 12 h. The cumulative release at 24 h reached 37.57 ± 2.12 %, which was significantly higher than that of the Free TIM group (10.38 ±

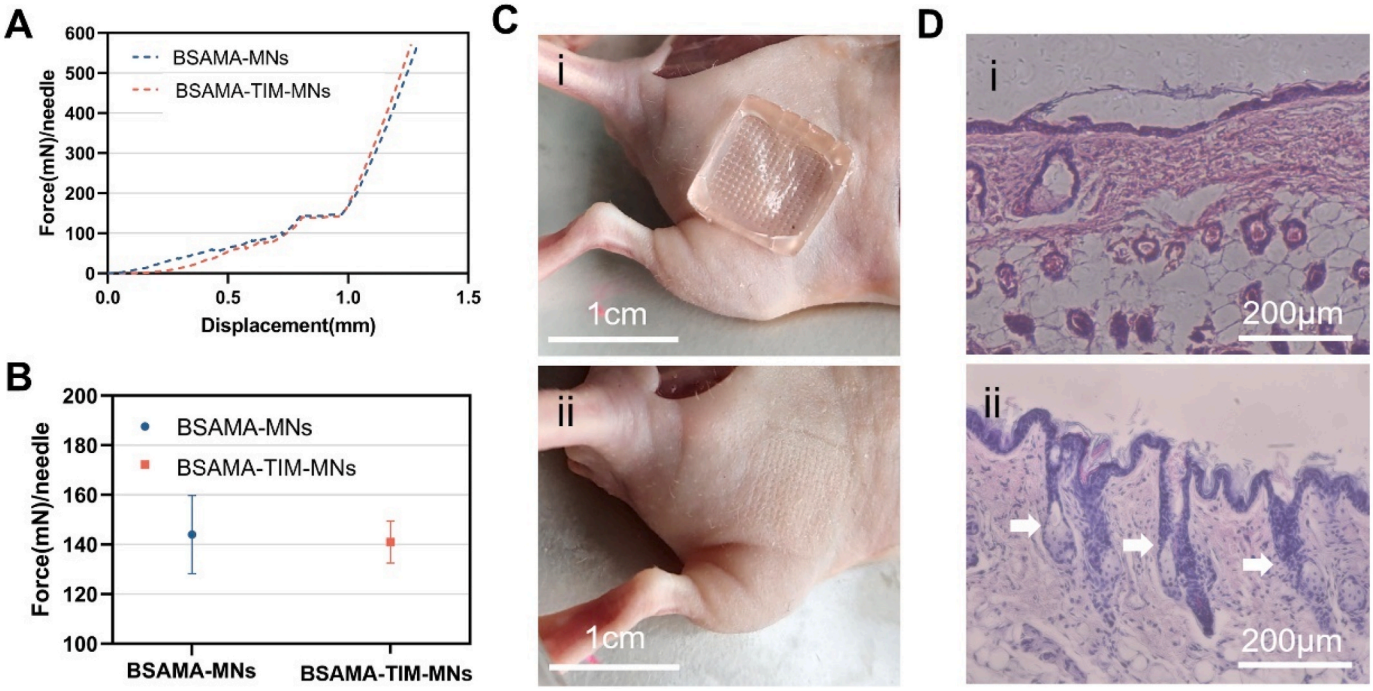

Fig. 2. Mechanical strength of microneedles: A) Force-displacement graph of the axial forces of the BSAMA-MNs and BSAMA-TIM-MNs, measured using a universal pressure testing machine; **B)** Failure forces of BSAMA-MNs and BSAMA-TIM-MNs; **C)** Mouse skin before **(i)** and after **(ii)** microneedle puncture. Scale bars: 1 cm; **D)** H & E staining of mouse skin before **(i)** and after **(ii)** microneedle puncture. Scale bars: 200 μm.

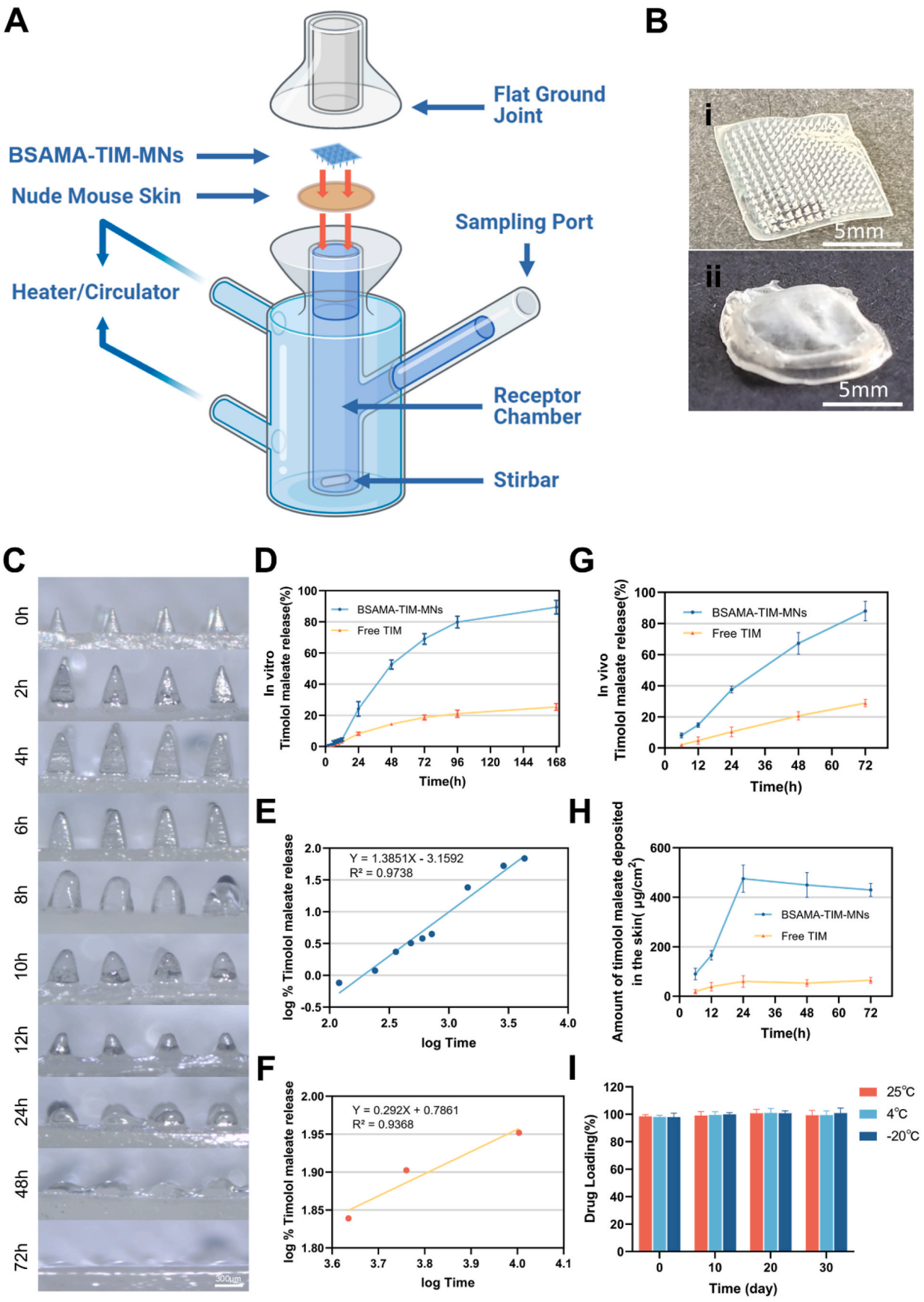

(caption on next page)

Fig. 3. Evaluation of the drug release capability of BSAMA microneedle patches loaded with timolol maleate. A) A schematic of the drug release process, which involves using nude mouse epidermis and a Franz diffusion cell to simulate microneedles during treatment; **B)** Digital images of the microneedles before **(i)** and after **(ii)** one week of the drug release experiment. Scale bars: 5 mm; **C)** Microneedle morphology at each time point of drug release. Scale bars: 300 μm; **D)** The *in vitro* release percentage-time graph of timolol maleate by hydrogel microneedle and traditional external application; **E), F)** Plots of log % cumulative release versus log time, according to the Korsmeyer-Peppas model for the first 72 h and 72–168 h, respectively. **G)** The *in vivo* release percentage-time graph of timolol maleate by hydrogel microneedle and traditional external application; **H)** Amount of timolol maleate deposited in the mice skin of hydrogel microneedle and traditional external application; **I)** Changes of timolol maleate content after hydrogel microneedle storage at three temperature conditions for 1 month.

3.13 %). By 72 h, 88.03 ± 6.25 % of the drug had been released through the MNs, approximately three times that of the Free TIM group (30.51 ± 7.98 %). Additionally, the detection of timolol maleate deposition in the skin revealed that the BSAMA-TIM-MNs group exceeded 100 μg/cm^2 at most time points, while the Free TIM group remained below 100 μg/cm^2 throughout the 72-h period (Fig. 3H). The experimental data confirmed that the skin drug retention of BSAMA-TIM-MNs was significantly higher than that of the Free TIM group at all time points, demonstrating its superior drug delivery efficiency.

3.4. Drug stability

To evaluate the drug stability of BSAMA-TIM-MNs under different storage conditions, the effective drug loading was analysed after storage at 25 °C, 4 °C, and −20 °C for 30 days. As shown in Fig. 3I, the effective drug content of timolol maleate in all storage temperature groups remained above 95 %, indicating that storage for 30 days at these three temperatures did not significantly affect the effective drug content of timolol maleate in the MNs. This suggests that the BSAMA material can provide a relatively stable environment for the loaded drug, thereby ensuring its chemical integrity during storage.

3.5. Cytotoxicity

The cytotoxicity of BSAMA was investigated because only BSAMA, which was used for the needle, entered the organism during the use of BSAMA-TIM-MNs. L929 cells were co-cultured with the BSAMA extract for 5 days. The cell viability (Fig. 4) remained >95 % on days 1, 3, and 5, indicating the biocompatibility of BSAMA MNs. Live/dead staining on days 1, 3, and 5 showed that L929 cells cultured with the BSAMA extract maintained normal viability throughout the entire test period. Additionally, there were no significant differences in cell morphology compared with control group. Notably, by day 5, both cell groups had reached contact inhibition, and no obvious dead cells were observed in either group.

3.6. Cell apoptosis assay

The live/dead cell staining (Fig. 5C) showed that after 24 h, there was no significant increase in the number of dead cells in the 3D cultures of HemECs treated with TIM compared to the control group. Compared to control group, TIM-treated HemECs showed the disappearance of filopodia, exhibited a rounded shape, and had a significant reduction in cell count, which was consistent with the results of the CCK-8 assay (Fig. 5A). TIM significantly inhibited HemEC growth in a concentration-dependent manner in both 3D and 2D cultures. In the 3D co-culture system, treatment with 900 μM TIM resulted in a cell inhibition rate of 44.12 ± 29.88 % over 24 h. In the 2D culture system, TIM concentrations <100 μM did not significantly inhibit the proliferation of HemECs, with a survival rate >92.95 ± 5.47 % (Fig. 5B). However, at concentrations >1 mM, the inhibition rate exceeded 50 %. The calculated half inhibitory concentration (IC50) was 794 μM at 24 h and 170 μM at 48 h.

3.7. Establishment of murine haemangioma model

Murine haemangioma models were established by the subcutaneous injection of HemECs and HUVECs into the backs of nude mice (Fig. 6A). Haemangiomas were observed 3 days after injection and gradually increased in size. At 15 d, the average volume of the haemangioma was 61.29 ± 23.84 mm^3 (Fig. 6B). No significant differences in body weight were observed (Fig. 6C). CD31 and GLUT-1 were used as specific biomarkers of IH to confirm haemangioma formation (Fig. 6D). Compared with the myocardium, CD31 and GLUT-1 expression was detected in the haemangioma tissue, confirming the successful establishment of the haemangioma model. The mice with successful modelling were randomly divided into 4 groups to study the antitumour effect (Fig. 6E).

3.8. Antitumour effects of BSAMA-TIM-MNs on murine haemangioma models

The tumour size was recorded after 15 days of treatment (Fig. 7A and B). Both the control and Free TIM groups showed haemangiomas protruding from the skin surface. Although the haemangiomas of the Free

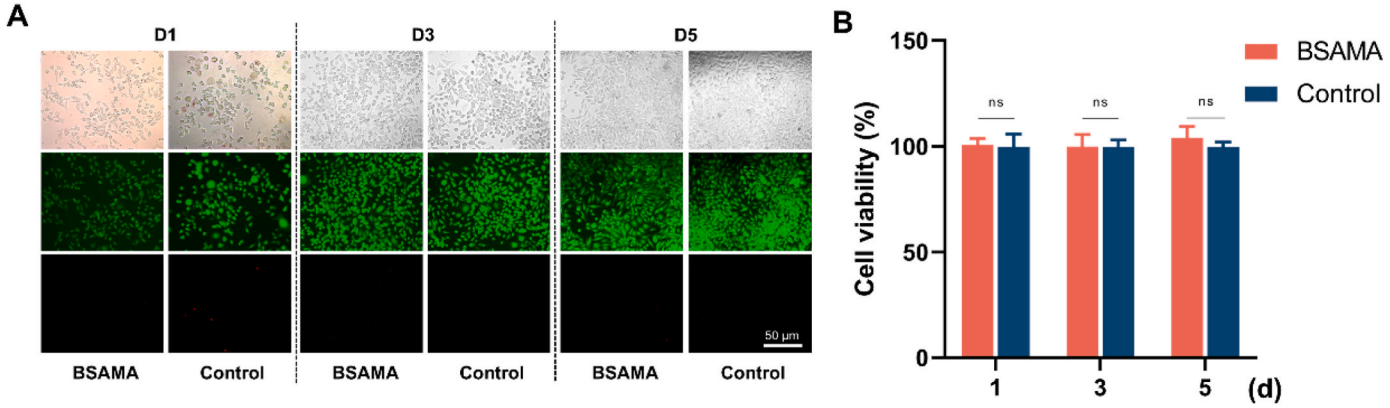

Fig. 4. Cytocompatibility testing of BSAMA using extraction solution method. A) Live/dead staining of L929 cells using fluorescence microscopy. Scale bars: 50 μm; **B)** Comparison of L929 survival rates between the complete culture medium and extract groups measured using CCK-8 reagent after culturing for 1, 3, and 5 days.

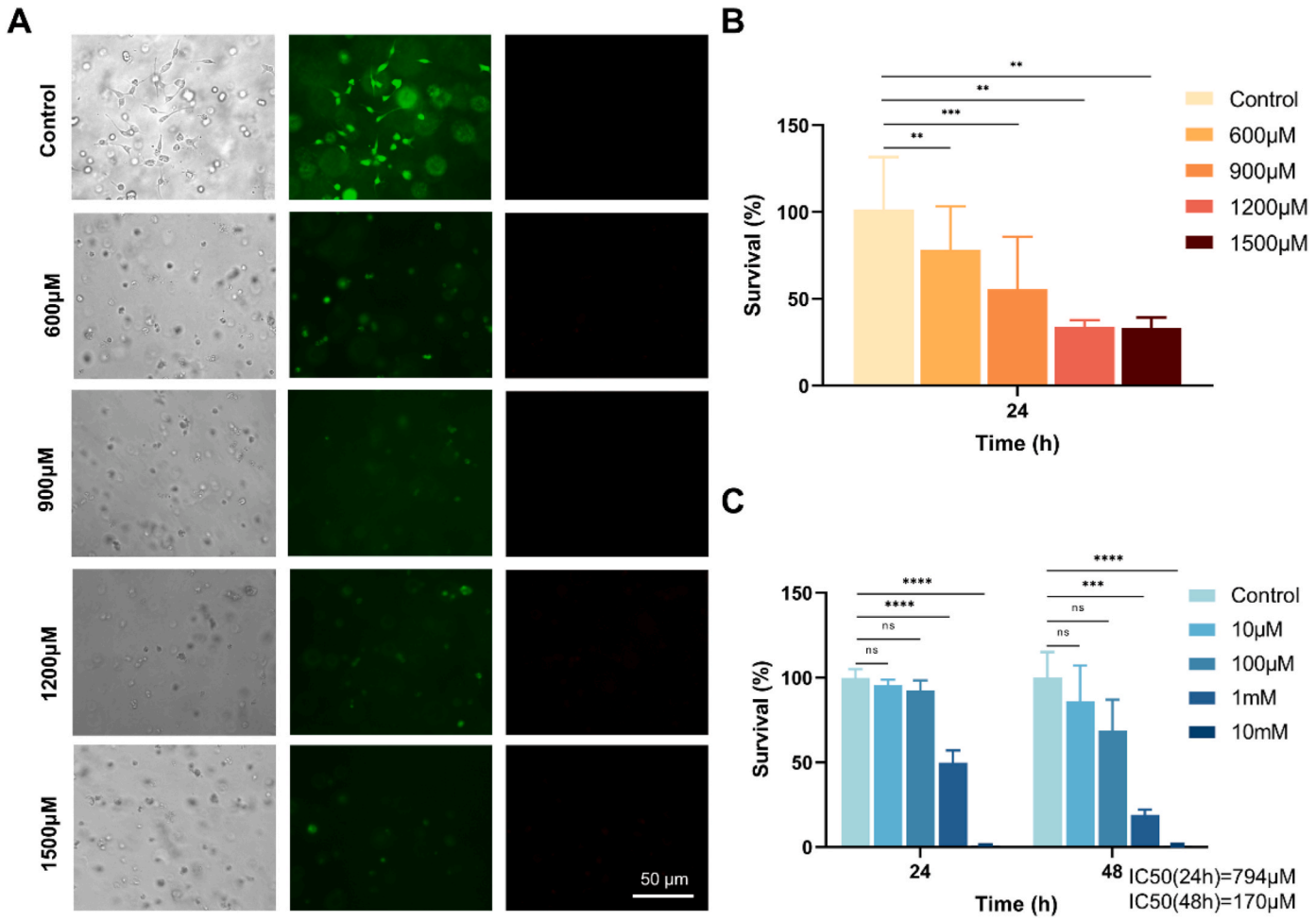

Fig. 5. The effects of timolol maleate on HemECs morphology and viability. A) Live-dead cell staining demonstrates the effects of different timolol maleate concentrations on the cell morphology of 3D-cultured HemECs. Scale bars: 50 μm; **B, C)** CCK-8 results of the influence of various timolol maleate concentrations on the cell viability of 2D- and 3D-cultured HemECs.

TIM group exhibited a slower growth with a reduced volume, the colour of the haemangiomas remained similar to that of the control group, with no significant fading. In contrast, the colour of the haemangiomas in the BSAMA-TIM-MNs group was lighter than those in both the Free TIM and control groups. Furthermore, the size of the haemangiomas in the BSAMA-TIM-MNs group showed a decreasing trend. Application of the BSAMA-TIM-MNs patch significantly controlled the haemangioma volume more effectively than either the BSAMA-MNs or Free TIM treatments. The control group showed a continuous increase in haemangioma size, with a gradually accelerating growth rate. The BSAMA-MNs group did not show a significant difference in haemangioma size compared with the control group. Although the Free TIM group exhibited a reduction in haemangioma volume compared to the control group, this reduction was considerably less pronounced than that observed in the BSAMA-TIM-MN group. Fig. 7C shows the images of the removed tumours. The tumour size in the BSAMA-TIM-MNs group was consistently smaller than that in the Free TIM group.

H & E staining of the haemangioma tissue (Fig. 7D) revealed a reduced number of microvessels in the BSAMA-TIM-MNs group compared to those in the other three groups. Additionally, large areas of vacuolated adipocytes were observed in the BSAMA-TIM-MNs group. Although some adipocytes were observed in the Free TIM group, their number was lower than that in the BSAMA-TIM-MNs group. Moreover, the density of the microvessels in the Free TIM group was higher than that in the BSAMA-TIM-MNs group.

The fluorescence intensity of GLUT-1 was weaker after treatment with BSAMA-TIM-MNs than in the other three groups (Fig. 7E and F). Western blot analysis (Fig. 7G) revealed that GLUT-1 expression was reduced by treatment with BSAMA-TIM-MNs and Free TIM. Notably, the relative GLUT-1 expression in the BSAMA-TIM-MNs group was significantly lower than that in the Free TIM group (Fig. 7H).

3.9. *In vivo biocompatibility of BSAMA-TIM-MNs*

Body weight increased over time in a similar manner in all groups (Fig. 8A). Fig. 8B shows representative images of the skin at the tumour site before and after MNs treatment and demonstrates that there was neither ulceration nor bleeding in the epidermis. H & E staining showed no structural changes in the lungs, liver, kidneys, heart, or spleen in any of the groups (Fig. 8C). Blood biochemical analyses showed that aspartate aminotransferase (AST) and uric acid (UA) levels did not change significantly (Fig. 8D).

4. Discussion

The major difficulty in the treatment of haemangiomas lies in insufficient drug at the tumour sites [50]. Most current clinical therapies attempt to address this problem by increasing the frequency of administration, which is, however, restricted by the limited availability of drugs [20]. Although topical timolol maleate (TIM) is non-invasive, both clinical studies and our own data show that it has three major limitations: low drug utilisation, local irritation, poor efficacy, and

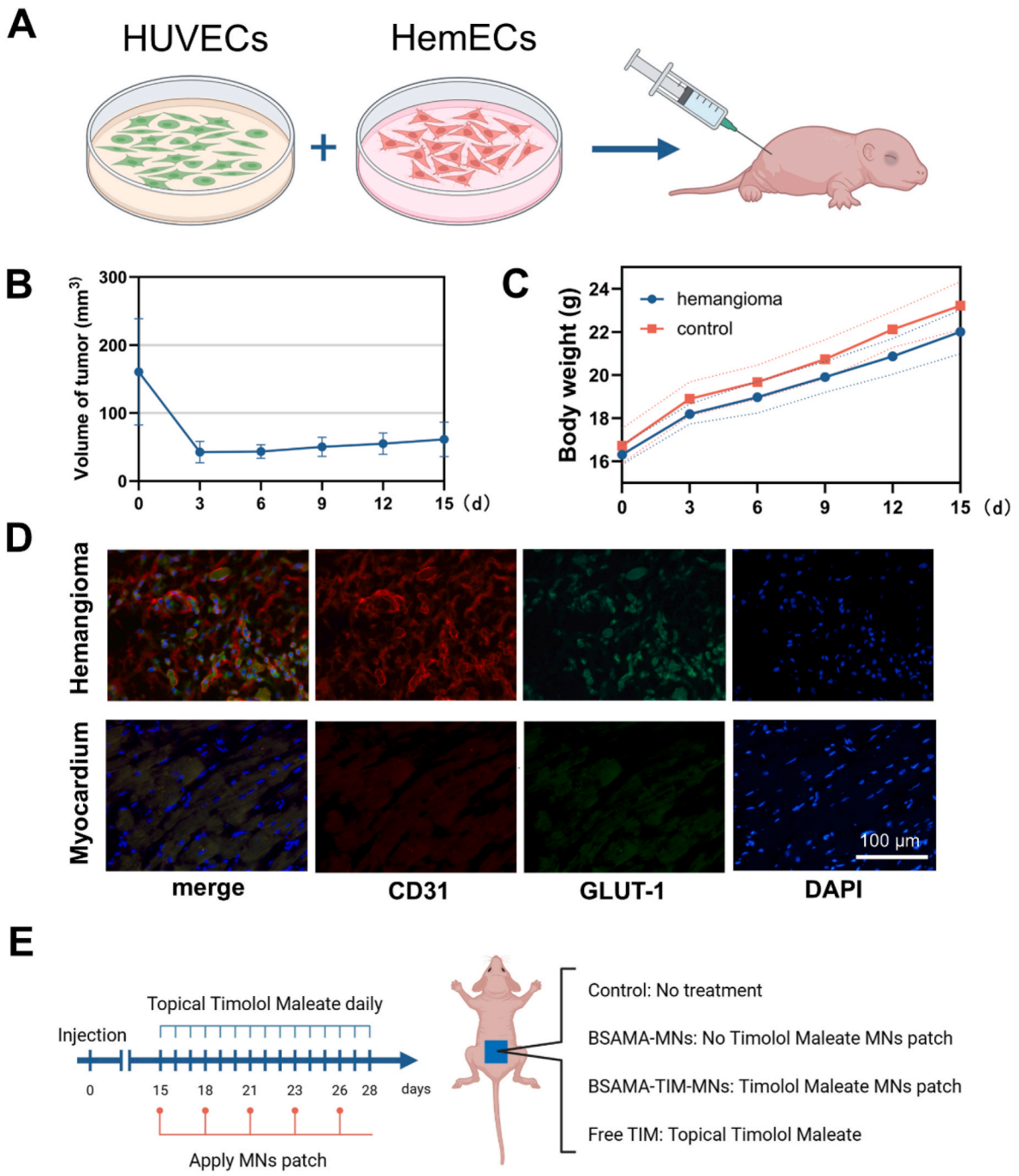

Fig. 6. Construction of haemangioma animal model by subcutaneous injection of cell suspensions into the backs of nude mice. A) Animal model of haemangioma is constructed by subcutaneous injection of HUVECs and HemECs mixed with Matrigel matrix into the backs of 4–5-week-old nude mice; **B)** After subcutaneous injections of cell suspensions into nude mice, the length and short diameter of the haemangioma were measured with a Vernier calliper every 3 days, and the volume was calculated to obtain the change in tumour volume in the first 2 weeks after modelling; **C)** Comparison of body weight between tumour-bearing and tumour-free nude mice within 2 weeks after modelling; **D)** Immunofluorescence staining of CD31 (red) and GLUT-1 (green) in mouse haemangioma and myocardial tissues. Scale bars: 100 μm; **E)** *In vivo* animal experiments and experimental grouping. The nude mice from the successfully constructed haemangioma model were divided into four groups: control, no treatment; BSAMA-MNs group, mice were treated with blank microneedle without timolol maleate every 3 days; Free TIM group, mice were administered with topical timolol maleate solution daily; and BSAMA-TIM-MNs group, mice were treated with microneedle containing timolol maleate every 3 days. (For interpretation of the references to colour in this figure legend, the reader is referred to the Web version of this article.)

inconsistent clinical outcomes. Due to its hydrophilic nature and the skin's natural barrier, only approximately 2–5 % of topically applied TIM can penetrate the stratum corneum. This means that the therapeutic concentration at the lesion site is insufficient [51]. Frequent applications (three times a day) and long-term use of topical TIM often cause skin irritation in infants, such as erythema and peeling. Moreover, suboptimal drug penetration makes it difficult to achieve complete regression of infantile IH [52]. Meta-analyses suggest that 20–30 % of IH cases do not respond well to topical TIM. In such cases, systemic therapies like oral propranolol are often required. However, these systemic treatments carry higher risks of systemic side effects [53]. Although widely explored, many MN platforms designed for systemic delivery,

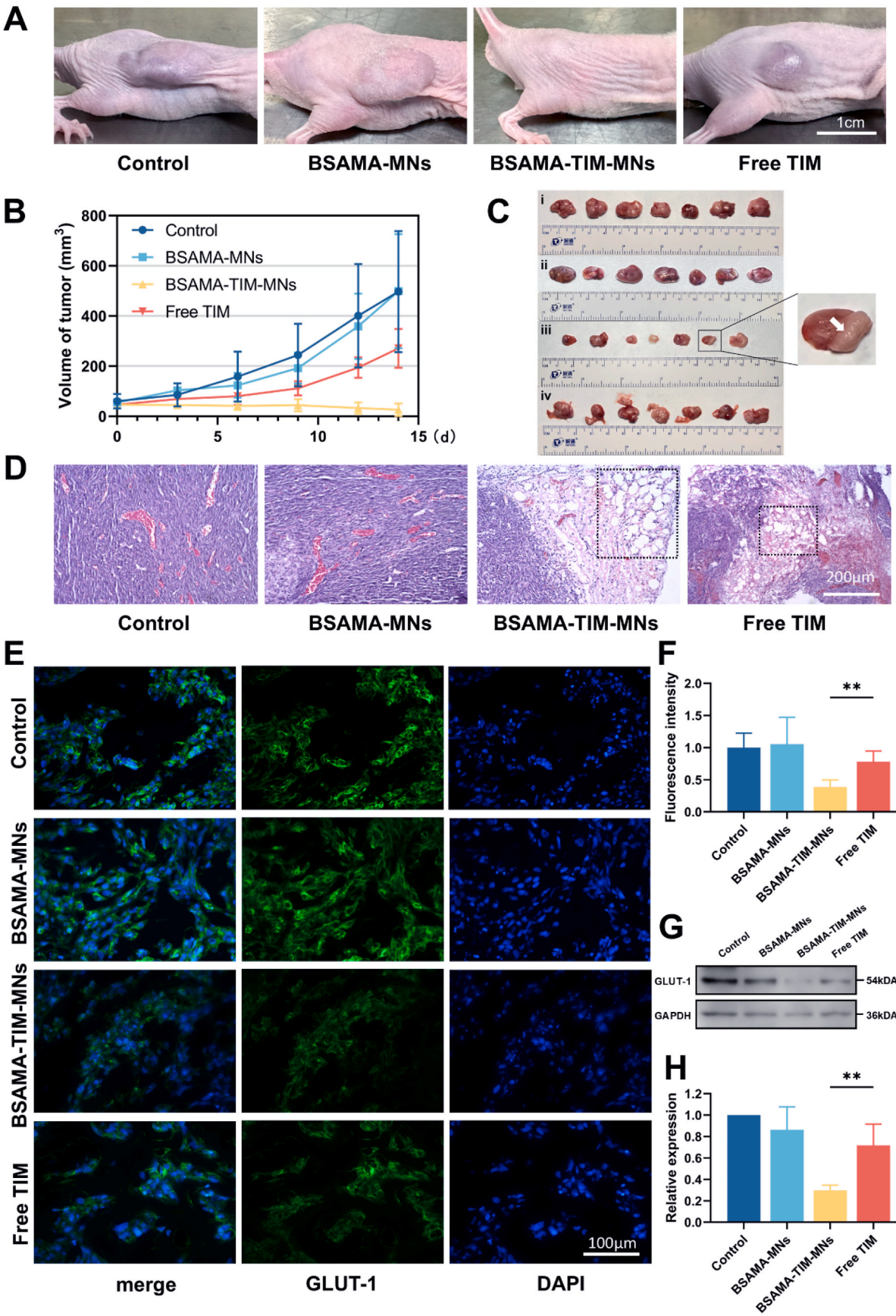

(caption on next page)

Fig. 7. ***In vivo*** **antitumour effects in haemangioma xenografts. A)** Animal models with haemangiomas and tumour grafts in the control, BSAMA-MNs, BSAMA-TIM-MNs, and Free TIM groups. Scale bars: 1 cm; **B)** Tumour volume changes in different groups during the 2-week treatment; **C)** Haemangiomas at the end of the 2-week experiment in the control **(i)**, BSAMA-MN **(ii)**, BSAMA-TIM-MNs **(iii)**, and Free TIM **(iv)** groups; **D)** H & E staining of hemangiomas and tumor grafts in the control, BSAMA-MNs, BSAMA-TIM-MNs, and Free TIM groups (Scale bars: 200 μm); **E)** Immunofluorescence images show the GLUT-1 expression in the control, BSAMA-MNs, BSAMA-TIM-MNs, and Free TIM groups (Scale bars: 100 μm); **F)** GLUT-1 fluorescence intensity in haemangioma tissues of four groups; **G)** Western blot analysis of GLUT1 expression in haemangioma tissues of each group after treatment. GAPDH was used as a loading control for intensity quantification; **H)** Relative GLUT-1 expression in the haemangioma tissues of the four groups.

like those used in vaccines, prioritize rapid dissolution. However, this is less than ideal for treating IH. In IH treatment, sustained local drug action is crucial. Most soluble MNs dissolve rapidly, often within less than 24 h. This results in an initial burst release, similar to a "high-dose shock", with over 50 % of the drug released within 6–12 h [54]. For diseases such as IH, which require a continuously maintained drug concentration at the lesion site during treatment, this uncontrolled rapid release can lead to systemic exposure risks and insufficient sustained efficacy. In this study, to offer a more effective alternative, we developed timolol-loaded BSAMA microneedles (BSAMA-TIM-MNs) to combine the high drug delivery rate of MNs with the anti-angiogenic and cytostatic capabilities of TIM. To the best of our knowledge, this is the first study to employ photocurable BSAMA for MN fabrication in IH therapy. BSAMA combines the biocompatibility of albumin with tunable photo-crosslinking, enabling mechanical strength optimization for robust skin penetration and gradual hydrogel degradation. Our data showed that the BSAMA-TIM-MNs group had a significantly lower tumour volume than the clinical Free TIM and control groups. Furthermore, immunofluorescence and western blot analyses showed significantly lower GLUT-1 expression in the BSAMA-TIM-MNs group than in the Free TIM and control groups. Our data suggest the promising application potential of BSAMA-TIM-MNs for tumour therapy in haemangiomas.

In this study, to treat superficial tumour haemangiomas, BSAMA-based MNs were utilised. BSAMA with a methacrylation degree of 97 % was used as the micro-nano storage material for TIM, owing to the swelling and compression modulus properties of BSAMA [43,45,55]. To ensure that the MNs patch conformed to the uneven body surfaces, we opted for PVA as the MNs substrate because of its exceptional toughness. As a promising transdermal drug delivery technique, MNs with lengths <1000 μm showed the highest delivery efficiency while painlessly and non-invasively piercing the dermis [56,57]. Studies have demonstrated that a base diameter of 200–300 μm, combined with a tip diameter of <50 μm, results in optimised mechanical properties for penetrating the stratum corneum [58]. Additionally, MNs with height-to-diameter ratios between 1.8 and 2.8 can prevent buckling and deformation [59]. Based on this, we used a customised mould with a needle length of 600 μm, base width of 300 μm (height-to-diameter ratio of 2.0), and tip diameter of 10 μm (Fig. 1) to prepare BSAMA MNs to improve the skin permeability to TIM. The pyramidal needle shape was selected because of the enhanced mechanical properties [60].

We tested the mechanical properties of MNs with and without TIM (Fig. 2A). These results indicate that the incorporation of TIM did not change the mechanical strength of the MNs. Based on previous studies, the minimum failure force required to pierce the skin efficiently is 45 mN/needle [61–63]. The safety factor (V), defined as the ratio of the failure force to the insertion force, is calculated as follows [63].

$$V = F_f / F_i \tag{1}$$

where F_f is the failure force of the MN tip, and F_i is the insertion force. In our study, the safety factors of BSAMA-MNs and BSAMA-TIM-MNs-were 3.2 (144 mN/45 mN) and 3.1 (141 mN/45 mN), respectively, which are both higher than the minimum safety factor of 2 required to safely penetrate the epidermis [61,62]. Furthermore, we applied the MNs to nude mouse skin (Fig. 2B), followed by H & E staining (Fig. 2C), and the results demonstrate the transdermal capacity of the MNs. This may be due to a high degree of substitution (DM) of BSAMA, which was 97 % in our study [45]. However, we observed that when BSAMA is used as the substrate material, the precursors are concentrated during MNs formation, leading to a reduction in flexibility (data not shown). This decreased flexibility negatively affects the adaptability of the MNs to the skin. Therefore, we chose biocompatible, flexible, and FDA-approved PVA as the substrate, which has good strength, elongation, tear resistance, flexibility, and recovery controllability [64].

We further characterised the release behaviour of BSAMA-TIM-MNs (Fig. 3). A slow-fast-slow drug release profile facilitates the continuous and stable delivery of TIM to tissues, which can further prevent angiogenesis and tumour cell proliferation at the haemangioma sites. One major advantage of BSAMA-TIM-MNs over the clinical gel patch (Free TIM) is its capacity to effectively release TIM to the haemangioma site. TIM is released via diffusion, swelling, and degradation of BSAMA and TIM during different periods [65]. To further explore the kinetics of TIM release, the release curve was fitted using the Korsmeyer–Peppas power model [66]:

$$M_t / M_\infty = \kappa t^n \tag{2}$$

$$\mathrm{Log}\, M_t / M_\infty = n \log t + \log \kappa \tag{3}$$

where M_t/M_∞ is defined as the fraction of drug released at time t, κ is a release constant, and n represents the release exponents. The value of n is determined from the slope of the plot of the logarithm of the release rate against the logarithm of time (t) (Equation (3)). Fig. 3E shows the kinetic exponent (n), coefficient of determination (R^2) and regression coefficient (r) values before and after 72 h. The release exponent (n), coefficient of determination (R^2) and regression coefficient (r) were 1.3851 and 0.9738, respectively, before 72 h, whereas after 72 h, the values were 0.292 for n and 0.9368 for R^2. This indicates that before 72 h, the release of TIM *in vitro* is governed by swelling, whereas after 72 h, diffusion becomes the primary mechanism. This is consistent with the swelling and degradation behaviour of BSAMA [43,45]. This result can also be verified by the morphological changes of the microneedles during the *in vitro* drug release process shown in Fig. 3C. Before 72 h, the tips of BSAMA did not degrade, and the release of TIM depended on the water absorption and swelling of BSAMA. After 72 h, BSAMA had basically degraded, and TIM was released from the tips of the needles to the epidermis, and then entered the subcutaneous tissue (i.e., the receiving chamber in the Franz diffusion cell) through the mechanism of free diffusion. The slow and continuous release of TIM ensures a high concentration at the site of the haemangioma lesions, thereby maintaining a sustained therapeutic effect. Notably, the *in vivo* release rate of TIM reached 88.03 ± 6.25 % at 72 h, which was significantly higher than the *in vitro* release rate of 69.02 ± 2.78 %. The possible reasons for this difference may be related to the enzymatic hydrolysis in the skin microenvironment and the accelerated drug diffusion caused by the flow of interstitial fluid. In addition, in the *in vitro* experiment, only the free TIM in the receiving chamber can be measured, while the TIM remaining in the epidermis of nude mice is ignored, which also leads to a lower result of the *in vitro* drug release rate.

The results showed that the drug retention rates of BSAMA-TIM-MNs remained above 95 % after 30 days of storage at −20 °C, 4 °C, and 25 °C (Fig. 3I). This property is critical for clinical applications, indicating that the formulation maintains drug activity under conventional storage conditions, addressing the degradation issues of traditional liquid TIM preparations. The protein matrix of BSAMA likely protects drug molecules through hydrophobic interactions and steric hindrance, preventing

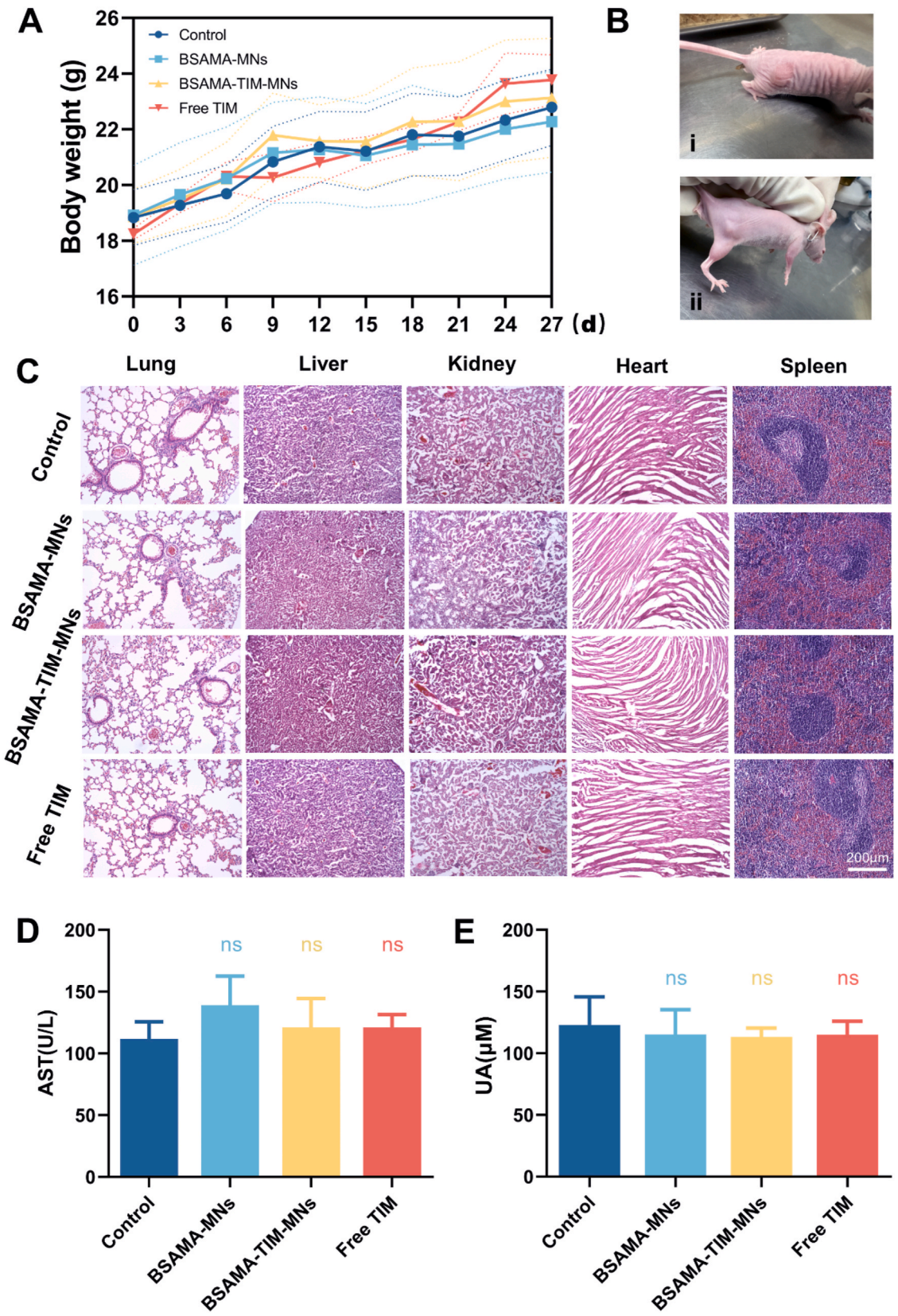

Fig. 8. ***In vivo*** **toxicity analysis in mice with haemangioma xenografts. A)** Body weights of tumour-burdened mice in different groups; **B)** Images of the epidermis of nude mice before **(i)** and after **(ii)** MNs therapy; **C)** Histopathologic imaging of the organs in tumour-burdened mice after treatments; **D)** Aspartate transaminase (AST) and uric acid (UA) levels in different groups after treatments. (*$p < 0.05$; **$p < 0.01$). Statistical differences were analysed by one-way analysis of variance and Bonferroni's post-hoc multiple comparisons. Scale bars: 200 μm.

hydrolysis or oxidation during storage. These findings provide experimental evidence for long-term storage and transportation of the product [67].

Recent findings have shown that some IH can regrow after discontinuing TIM treatment, although the underlying mechanism remains unclear [68,69]. One of the mechanisms of TIM in haemangiomas is the inhibition of HemEC proliferation [70]. In the present study, HemECs cultured in 3D and 2D models were treated with different TIM concentrations to test this hypothesis. The results indicate that TIM can effectively inhibit HemEC proliferation in a dose-dependent manner, providing guidance for determining the appropriate TIM dosage in MNs. This allows the amount of drug in the MNs to be therapeutic without overdosing. However, the molecular mechanism underlying the induction of cell apoptosis by BSAMA-TIM-MNs requires further investigation.

To investigate whether the BSAMA-TIM-MNs could eliminate haemangiomas *in vivo*, a rude mouse model was adopted (Fig. 6) via subcutaneous injection of pluripotent HemECs supplemented with HUVECs, based on the following considerations: 1) endothelial cell vascular formation is the common component among the three stages of haemangioma formation, which include the initial phase of rapid proliferation, the transition phase of slow involution, and the final phase of complete regression; 2) HUVECs can improve the vascularization and increase the expression of a haemangioma specific marker GLUT-1, due to its stem cell potential [71]; 3) the cycle of haemangioma formation is shortened by supplementary HUVECs [72]; and 4) HemECs are more easily obtained than HemSCs, which require a specific magnetic cell separation [73]. Our results (Fig. 6D) show that the modelled haemangioma form a large number of new blood vessels and that the CD31-positive endothelial cells are human-derived, indicating the successful establishment of the *in vivo* haemangioma model.

Our results indicate that the haemangioma entered the phase of involution (i.e., few remaining capillary-like vessels surrounded by loose fibrofatty tissue [74]) in the Free TIM and BSAMA-TIM-MNs groups, whereas it remained in the proliferation phase (i.e., large numbers of proliferating endothelial cells [75]) in the control and BSAMA-MNs groups. There was no significant difference in haemangioma size between the control and BSAMA-MNs groups, indicating that the therapeutic effect in the BSAMA-TIM-MNs group is not attributable to MNs compression. Moreover, research has shown that the evaluation of the therapeutic effects on haemangiomas primarily relies on changes in size, colour, depth, and functional damage to the tumour tissue [76]. Among these indicators, changes in lesion colour and size are particularly crucial for assessing therapeutic effects. This suggests that although Free TIM has a therapeutic effect, it slows down the growth rate of the haemangioma but does not reduce its size, whereas BSAMA-TIM-MNs eliminate the haemangioma. This enhanced therapeutic effect is attributable to the sustained and effective delivery of TIM to the surrounding IH tissue by the BSAMA-TIM-MNs, even at lower dosing frequencies and amounts. The expression of GLUT-1 in the haemangioma tissues of the BSAMA-TIM-MNs treatment group was significantly reduced, (Fig. 7E–H), which is consistent with H&E staining showing decreased vascular density and adipocyte replacement (Fig. 7D). As a specific marker of haemangioma endothelial cells, GLUT-1 downregulation suggests that TIM may induce endothelial cell apoptosis by inhibiting glucose metabolism pathways. BSAMA-TIM-MNs does not only enhance the transdermal delivery efficiency of TIM and promote drug absorption by haemangioma tissue but also help avoid potential adverse reactions from oral administration. This innovative approach potentially offers a new clinical treatment method for IH and serves as a versatile drug delivery platform with broad applications in clinical practice.

5. Conclusion

In this study, we developed BSAMA-TIM-MNs as a promising TIM delivery system with a potent capacity to reduce the size and volume of haemangiomas and decrease GLUT-1 expression. The BSAMA-TIM-MNs show mechanical strength with sustained TIM release. Compared with the clinical Free TIM group, BSAMA-TIM-MNs show better therapeutic effects with lower administration frequencies and dosages. Furthermore, MNs do not cause skin ulcers or bleeding and do not produce toxic side effects in the body. TIM therapy based on the BSAMA-MNs release system may improve the therapeutic efficacy and reduce the dose and frequency of TIM administration, providing a promising strategy for the treatment of IH.

CRediT authorship contribution statement

Xiaokun Lin: Writing – original draft, Methodology, Formal analysis, Data curation. **Tongshuai Kuang:** Writing – original draft, Methodology, Formal analysis, Data curation. **Lei Wang:** Writing – review & editing, Conceptualization. **Wei Cai:** Methodology. **Linxing Yang:** Formal analysis, Data curation. **Changrong Guo:** Formal analysis, Data curation. **Xinyang Pan:** Formal analysis, Data curation. **Yuanhao Wang:** Formal analysis, Data curation. **Qiang Gao:** Formal analysis, Data curation. **Kaihui Nan:** Conceptualization. **Lingli Li:** Writing – review & editing, Conceptualization.

Declaration of competing interest

The authors declare that there are no conflicts of interest regarding the publication of this manuscript. We confirm that there are no financial or personal relationships that could inappropriately influence our work. All funding sources and support received for this research have been disclosed in the manuscript.

Acknowledgements

This study was funded by the Wenzhou Science and Technology Foundation (Y20210266), Natural Science Foundation of Zhejiang Province (LY24C100002), a start-up grant from the Wenzhou Institute, University of Chinese Academy of Sciences (WIUCAS, WIUCASQD2023022, WIUCASQD2022035), Zhejiang Engineering Research Center for Tissue Repair Materials, WIUCAS (WIUCASZZXF21002), Wenzhou Key Laboratory of Biomaterials and Engineering, WIUCAS (WIUCASSWCL21003), and Joint Medical Research Center of Xiangshan Hospital Affiliated to Wenzhou Medical University and WIUCAS (WIUCASXSZX09).

Data availability

Data will be made available on request.

References

[1] C. Léauté-Labrèze, J.I. Harper, P.H. Hoeger, Infantile haemangioma, Lancet 390 (2017) 85–94, https://doi.org/10.1016/s0140-6736(16)00645-0.
[2] T. Itinteang, A.H. Withers, P.F. Davis, S.T. Tan, Biology of infantile hemangioma, Front Surg 1 (2014) 38, https://doi.org/10.3389/fsurg.2014.00038.
[3] P.A. Laken, Infantile hemangiomas: pathogenesis and review of propranolol use, Adv. Neonatal Care 16 (2016) 135–142, https://doi.org/10.1097/anc.0000000000000254.
[4] J.I. Ademola, C.A. Chow, R.C. Wester, H.I. Maibach, Metabolism of propranolol during percutaneous absorption in human skin, J. Pharmaceut. Sci. 82 (1993) 767–770, https://doi.org/10.1002/jps.2600820802.
[5] E. Fernández Faith, et al., Incidence and clinical factors associated with ulceration in infantile hemangiomas, J. Am. Acad. Dermatol. 88 (2023) 414–420, https://doi.org/10.1016/j.jaad.2022.10.047.
[6] Y. Ji, S. Chen, K. Li, L. Li, C. Xu, B. Xiang, Signaling pathways in the development of infantile hemangioma, J. Hematol. Oncol. 7 (2014) 13, https://doi.org/10.1186/1756-8722-7-13.
[7] K.R. Satterfield, C.B. Chambers, Current treatment and management of infantile hemangiomas, Surv. Ophthalmol. 64 (2019) 608–618, https://doi.org/10.1016/j.survophthal.2019.02.005.
[8] A. Langley, E. Pope, Propranolol and central nervous system function: potential implications for paediatric patients with infantile haemangiomas, Br. J. Dermatol. 172 (2015) 13–23, https://doi.org/10.1111/bjd.13379.

[9] A.V. Moyakine, J.M. Kerstjens, S. Spillekom-van Koulil, C.J. van der Vleuten, Propranolol treatment of infantile hemangioma (IH) is not associated with developmental risk or growth impairment at age 4 years, J. Am. Acad. Dermatol. 75 (2016) 59–63.e51, https://doi.org/10.1016/j.jaad.2016.02.1218.

[10] J.M.C. Tan, H.W. Lim, M.J. Koh, Oral propranolol for the treatment of infantile haemangiomas in Singapore, Singap. Med. J. 62 (2021) 139–142, https://doi.org/10.11622/smedj.2020008.

[11] S. Shah, I.J. Frieden, Treatment of infantile hemangiomas with beta-blockers: a review, Skin Therapy Lett 18 (2013) 5–7.

[12] L. Zheng, Y. Li, Effect of topical timolol on response rate and adverse events in infantile hemangioma: a meta-analysis, Arch. Dermatol. Res. 310 (2018) 261–269, https://doi.org/10.1007/s00403-018-1815-y.

[13] K.M. Saari, P.J. Airaksinen, E.A. Jaanio, Hypotensive effect of timolol on secondary glaucoma in chronic uveitis, Lancet 1 (1978) 442, https://doi.org/10.1016/s0140-6736(78)91228-x.

[14] H. Philippin, et al., Selective laser trabeculoplasty versus 0·5% timolol eye drops for the treatment of glaucoma in Tanzania: a randomised controlled trial, Lancet Global Health 9 (2021) e1589–e1599, https://doi.org/10.1016/s2214-109x(21)00348-x.

[15] X. Wang, W. Feng, X. Zhao, Z. Liu, L. Dong, The efficacy and safety of topical β-blockers in treating infantile hemangiomas: a meta-analysis including 11 randomized controlled trials, Dermatology 237 (2021) 433–443, https://doi.org/10.1159/000510029.

[16] M. Alzaid, A. Al-Naseem, F. Al-Niaimi, F.R. Ali, Topical timolol in dermatology: infantile haemangiomas and beyond, Clin. Exp. Dermatol. 47 (2022) 819–832, https://doi.org/10.1111/ced.15021.

[17] C.B. Chambers, W.R. Katowitz, J.A. Katowitz, G. Binenbaum, A controlled study of topical 0.25% timolol maleate gel for the treatment of cutaneous infantile capillary hemangiomas, Ophthalmic Plast. Reconstr. Surg. 28 (2012) 103–106, https://doi.org/10.1097/IOP.0b013e31823bfffb.

[18] N. Ni, P. Langer, R. Wagner, S. Guo, Topical timolol for periocular hemangioma: report of further study, Arch. Ophthalmol. 129 (2011) 377–379, https://doi.org/10.1001/archophthalmol.2011.24.

[19] L. Yu, et al., Treatment of superficial infantile hemangiomas with timolol: evaluation of short-term efficacy and safety in infants, Exp. Ther. Med. 6 (2013) 388–390, https://doi.org/10.3892/etm.2013.1176.

[20] Y. Qiu, M. Chen, L. Chang, G. Ma, X.Hu, Y. Jin, H. Chen, X. Lin, Effect of timolol maleate gel-forming solution in the treatment of superficial infantile hemangiomas: a prospective, randomized, double-blind, controlled trial, J. Tiss. Eng. Reconstructive Surgery 10 (2014) 203-206.

[21] S. Zhang, C. Liu, Y. Song, J. Ruan, P. Quan, L. Fang, High drug-loading and controlled-release hydroxyphenyl-polyacrylate adhesive for transdermal patch, J. Contr. Release 353 (2023) 475–489, https://doi.org/10.1016/j.jconrel.2022.11.058.

[22] W. Hu, et al., Hyaluronidase-powered microneedles for significantly enhanced transdermal delivery efficiency, J. Contr. Release 353 (2023) 380–390, https://doi.org/10.1016/j.jconrel.2022.11.046.

[23] T. Liang, X. Liu, Y. Tong, Q. Ding, M. Yang, H. Ning, Recent advances in targeted therapies for infantile hemangiomas, Int. J. Nanomed. 6127–6143 (2024).

[24] Q. Jiao, et al., Studies on stratum corneum metabolism: function, molecular mechanism and influencing factors, J. Cosmet. Dermatol. 21 (2022) 3256–3264, https://doi.org/10.1111/jocd.15000.

[25] G.N. Stamatas, P.F. Roux, E. Boireau-Adamezyk, I. Lboukili, T. Oddos, Skin maturation from birth to 10 years of age: structure, function, composition and microbiome, Exp. Dermatol. 32 (2023) 1420–1429, https://doi.org/10.1111/exd.14843.

[26] D.A. Lintzeri, N. Karimian, U. Blume-Peytavi, J. Kottner, Epidermal thickness in healthy humans: a systematic review and meta-analysis, J. Eur. Acad. Dermatol. Venereol. 36 (2022) 1191–1200, https://doi.org/10.1111/jdv.18123.

[27] H. Wu, X. Wang, H. Liang, J. Zheng, S. Huang, D. Zhang, Enhanced efficacy of propranolol therapy for infantile hemangiomas based on a mesoporous silica nanoplatform through mediating autophagy dysfunction, Acta Biomater. 107 (2020) 272–285, https://doi.org/10.1016/j.actbio.2020.02.033.

[28] M.R. Prausnitz, R. Langer, Transdermal drug delivery, Nat. Biotechnol. 26 (2008) 1261–1268, https://doi.org/10.1038/nbt.1504.

[29] M. Gupta, U. Agrawal, S.P. Vyas, Nanocarrier-based topical drug delivery for the treatment of skin diseases, Expet Opin. Drug Deliv. 9 (2012) 783–804, https://doi.org/10.1517/17425247.2012.686490.

[30] D. Yang, et al., Microneedle-mediated transdermal drug delivery for treating diverse skin diseases, Acta Biomater. 121 (2021) 119–133, https://doi.org/10.1016/j.actbio.2020.12.004.

[31] R.K. Kankala, et al., Highly porous microcarriers for minimally invasive in situ skeletal muscle cell delivery, Small 15 (2019) e1901397, https://doi.org/10.1002/smll.201901397.

[32] M. Jeyhani, S.Y. Mak, S. Sammut, H.C. Shum, D.K. Hwang, S.S.H. Tsai, Controlled electrospray generation of nonspherical alginate microparticles, ChemPhysChem 19 (2018) 2113–2118, https://doi.org/10.1002/cphc.201701094.

[33] S. Hassan, et al., Evolution and clinical translation of drug delivery nanomaterials, Nano Today 15 (2017) 91–106, https://doi.org/10.1016/j.nantod.2017.06.008.

[34] J.G. Turner, L.R. White, P. Estrela, H.S. Leese, Hydrogel-Forming microneedles: current advancements and future trends, Macromol. Biosci. 21 (2021) e2000307, https://doi.org/10.1002/mabi.202000307.

[35] M.J. Kim, et al., Minoxidil-loaded hyaluronic acid dissolving microneedles to alleviate hair loss in an alopecia animal model, Acta Biomater. 143 (2022) 189–202, https://doi.org/10.1016/j.actbio.2022.02.011.

[36] Y. Chi, et al., Enzyme-mediated fabrication of nanocomposite hydrogel microneedles for tunable mechanical strength and controllable transdermal efficiency, Acta Biomater. 174 (2024) 127–140, https://doi.org/10.1016/j.actbio.2023.11.038.

[37] Y. Zheng, et al., Separable nanocomposite hydrogel microneedles for intradermal and sustained delivery of antigens to enhance adaptive immune responses, Acta Biomater. 185 (2024) 203–214, https://doi.org/10.1016/j.actbio.2024.07.031.

[38] M. Xu, N. Mehwish, B.H. Lee, Facile fabrication of transparent and opaque albumin methacryloyl gels with highly improved mechanical properties and controlled pore structures, Gels 8 (2022), https://doi.org/10.3390/gels8060367.

[39] C.C. Hsu, A. Serio, N. Amdursky, C. Besnard, M.M. Stevens, Fabrication of hemin-doped serum albumin-based fibrous scaffolds for neural tissue engineering applications, ACS Appl. Mater. Interfaces 10 (2018) 5305–5317, https://doi.org/10.1021/acsami.7b18179.

[40] N. Mehwish, M. Xu, M. Zaeem, B.H. Lee, Mussel-inspired surface functionalization of porous albumin cryogels supporting synergistic antibacterial/antioxidant activity and bone-like apatite formation, Gels 8 (2022), https://doi.org/10.3390/gels8100679.

[41] K. Duan, et al., Autoclavable albumin-based cryogels with uncompromising properties, Gels 9 (2023), https://doi.org/10.3390/gels9090712.

[42] J. Ong, J. Zhao, A.W. Justin, A.E. Markaki, Albumin-based hydrogels for regenerative engineering and cell transplantation, Biotechnol. Bioeng. 116 (2019) 3457–3468, https://doi.org/10.1002/bit.27167.

[43] Y. Chen, et al., Comparison of globular albumin methacryloyl and random-coil gelatin methacryloyl: preparation, hydrogel properties, cell behaviors, and mineralization, Int. J. Biol. Macromol. 204 (2022) 692–708, https://doi.org/10.1016/j.ijbiomac.2022.02.028.

[44] D. Lantigua, et al., Synthesis and characterization of photocrosslinkable albumin-based hydrogels for biomedical applications, Soft Matter 16 (2020) 9242–9252, https://doi.org/10.1039/d0sm00977f.

[45] G. Ferracci, et al., Photocurable albumin methacryloyl hydrogels as a versatile platform for tissue engineering, ACS Appl. Bio Mater. 3 (2020) 920–934, https://doi.org/10.1021/acsabm.9b00984.

[46] K. Zhang, et al., Application of polyvinyl alcohol/chitosan copolymer hydrogels in biomedicine: a review, Int. J. Biol. Macromol. 242 (2023) 125192, https://doi.org/10.1016/j.ijbiomac.2023.125192.

[47] M.S. El-Okaily, et al., Efficient drug delivery vehicles of environmentally benign nano-fibers comprising bioactive glass/chitosan/polyvinyl alcohol composites, Int. J. Biol. Macromol. 182 (2021) 1582–1589, https://doi.org/10.1016/j.ijbiomac.2021.05.079.

[48] S.G. Jin, Production and application of biomaterials based on polyvinyl alcohol (PVA) as wound dressing, Chem. Asian J. 17 (2022) e202200595, https://doi.org/10.1002/asia.202200595.

[49] R. Zhang, D. Zhang, X. Sun, X. Song, K.C. Yan, H. Liang, Polyvinyl alcohol/gelatin hydrogels regulate cell adhesion and chromatin accessibility, Int. J. Biol. Macromol. 219 (2022) 672–684, https://doi.org/10.1016/j.ijbiomac.2022.08.025.

[50] F.Z. Muñoz-Garza, et al., Efficacy and safety of topical timolol for the treatment of infantile hemangioma in the early proliferative stage: a randomized clinical trial, JAMA Dermatol. 157 (2021) 583–587, https://doi.org/10.1001/jamadermatol.2021.0596.

[51] S. Chinnadurai, et al., Pharmacologic interventions for infantile hemangioma: a meta-analysis, Pediatrics 137 (2016).

[52] C. Léauté-Labrèze, et al., A randomized, controlled trial of oral propranolol in infantile hemangioma, N. Engl. J. Med. 372 (2015) 735–746.

[53] X. Huang, et al., Efficacy and safety of oral propranolol and topical timolol in the treatment of infantile hemangioma: a meta-analysis and systematic review, Front. Pharmacol. 15 (2024) 1515901.

[54] H. Jiang, et al., Oxidized cellulose microneedle patch combined with vascular embolization and local delivery of timolol maleate for hemangiomas, Colloids Surf. B Biointerfaces 244 (2024) 114174, https://doi.org/10.1016/j.colsurfb.2024.114174.

[55] N. Mehwish, Y. Chen, M. Zaeem, Y. Wang, B.H. Lee, H. Deng, Novel biohybrid spongy scaffolds for fabrication of suturable intraoral graft substitutes, Int. J. Biol. Macromol. 214 (2022) 617–631, https://doi.org/10.1016/j.ijbiomac.2022.06.125.

[56] J.M. Loh, Y.J.L. Lim, J.T. Tay, H.M. Cheng, H.L. Tey, K. Liang, Design and fabrication of customizable microneedles enabled by 3D printing for biomedical applications, Bioact. Mater. 32 (2024) 222–241, https://doi.org/10.1016/j.bioactmat.2023.09.022.

[57] Y. Zuo, R. Sun, N. Del Piccolo, M.M. Stevens, Microneedle-mediated nanomedicine to enhance therapeutic and diagnostic efficacy, Nano Converg 11 (2024) 15, https://doi.org/10.1186/s40580-024-00421-w.

[58] X. Luo, L. Yang, Y. Cui, Microneedles: materials, fabrication, and biomedical applications, Biomed. Microdevices 25 (2023) 20, https://doi.org/10.1007/s10544-023-00658-y.

[59] D. Ando, et al., Mechanical characterization of dissolving microneedles: factors affecting physical strength of needles, Pharmaceutics 16 (2024), https://doi.org/10.3390/pharmaceutics16020200.

[60] G. Anbazhagan, S.B. Suseela, R. Sankararajan, Design, analysis and fabrication of solid polymer microneedle patch using CO(2) laser and polymer molding, Drug Deliv Transl Res 13 (2023) 1813–1827, https://doi.org/10.1007/s13346-023-01296-w.

[61] J.H. Park, M.G. Allen, M.R. Prausnitz, Polymer microneedles for controlled-release drug delivery, Pharm. Res. 23 (2006) 1008–1019, https://doi.org/10.1007/s11095-006-0028-9.

[62] M.A. Lopez-Ramirez, et al., Built-in active microneedle patch with enhanced autonomous drug delivery, Adv. Mater. 32 (2020) e1905740, https://doi.org/10.1002/adma.201905740.
[63] S.P. Davis, B.J. Landis, Z.H. Adams, M.G. Allen, M.R. Prausnitz, Insertion of microneedles into skin: measurement and prediction of insertion force and needle fracture force, J. Biomech. 37 (2004) 1155–1163, https://doi.org/10.1016/j.jbiomech.2003.12.010.
[64] Y. Chen, J. Song, S. Wang, W. Liu, PVA-based hydrogels: promising candidates for articular cartilage Repair, Macromol. Biosci. 21 (2021) e2100147, https://doi.org/10.1002/mabi.202100147.
[65] B.Z. Chen, et al., Strategies to develop polymeric microneedles for controlled drug release, Adv. Drug Deliv. Rev. 203 (2023) 115109, https://doi.org/10.1016/j.addr.2023.115109.
[66] C. Maderuelo, A. Zarzuelo, J.M. Lanao, Critical factors in the release of drugs from sustained release hydrophilic matrices, J. Contr. Release 154 (2011) 2–19, https://doi.org/10.1016/j.jconrel.2011.04.002.
[67] A. Rignall, ICHQ1A (R2) stability testing of new drug substance and product and ICHQ1C stability testing of new dosage forms. ICH Quality Guidelines: an Implementation Guide, 2017, pp. 3–44.
[68] L. Bagazgoitia, Á. Hernández-Martín, A. Torrelo, Recurrence of infantile hemangiomas treated with propranolol, Pediatr. Dermatol. 28 (2011) 658–662, https://doi.org/10.1111/j.1525-1470.2011.01644.x.
[69] Q. Xiao, Q. Li, B. Zhang, W. Yu, Propranolol therapy of infantile hemangiomas: efficacy, adverse effects, and recurrence, Pediatr. Surg. Int. 29 (2013) 575–581, https://doi.org/10.1007/s00383-013-3283-y.
[70] H. Zhu, H. Luo, W. Lai, Efficacy of timolol in the treatment of facial hemangioma and its effect on the proliferation and apoptosis of hemangioma stem cells, Cell Mol Biol (Noisy-le-grand) 69 (2023) 115–120, https://doi.org/10.14715/cmb/2023.69.10.16.
[71] E. Yang, et al., Shikonin reverses pyruvate kinase isoform M2-mediated propranolol resistance in infantile hemangioma through reactive oxygen species-induced autophagic dysfunction, Cancer Sci. 114 (2023) 806–821, https://doi.org/10.1111/cas.15649.
[72] M. Kong, Y. Li, K. Wang, S. Zhang, Y. Ji, Infantile hemangioma models: is the needle in a haystack? J. Transl. Med. 21 (2023) 308, https://doi.org/10.1186/s12967-023-04144-0.
[73] L. Huang, J. Bischoff, Isolation of stem cells, endothelial cells and pericytes from human infantile hemangioma, Bio Protoc 10 (2020) e3487, https://doi.org/10.21769/BioProtoc.3487.
[74] Y. Yu, et al., Mesenchymal stem cells and adipogenesis in hemangioma involution, Stem Cell. 24 (2006) 1605–1612, https://doi.org/10.1634/stemcells.2005-0298.
[75] K. Takahashi, J.B. Mulliken, H.P. Kozakewich, R.A. Rogers, J. Folkman, R. A. Ezekowitz, Cellular markers that distinguish the phases of hemangioma during infancy and childhood, J. Clin. Investig. 93 (1994) 2357–2364, https://doi.org/10.1172/jci117241.
[76] H. Wu, et al., Propranolol-loaded mesoporous silica nanoparticles for treatment of infantile hemangiomas, Adv Healthc Mater 8 (2019) e1801261, https://doi.org/10.1002/adhm.201801261.